Geophysical Research Letters

RESEARCH LETTER
10.1029/2019GL084878

**Key Points:**
- The QBO becomes realistic in historical and decadal hindcast simulations when the external forcing data are changed from CMIP5 to CMIP6
- In the first three lead years, the forecast skill of the QBO is increased after the initialization of the decadal hindcasts with observations
- Evidence is found that the update of the ozone data in CMIP6 leads to the realistic QBO variability

**Supporting Information:**
- Supporting Information S1

**Correspondence to:**
H. Pohlmann,
holger.pohlmann@mpimet.mpg.de

**Citation:**
Pohlmann, H., Müller, W. A., Bittner, M., Hettrich, S., Modali, K., Pankatz, K., & Marotzke, J. (2019). Realistic quasi-biennial oscillation variability in historical and decadal hindcast simulations using CMIP6 forcing. *Geophysical Research Letters*, *46*, 14,118–14,125. https://doi.org/10.1029/2019GL084878

Received 7 AUG 2019
Accepted 19 NOV 2019
Accepted article online 20 NOV 2019
Published online 3 DEC 2019



# Realistic Quasi-Biennial Oscillation Variability in Historical and Decadal Hindcast Simulations Using CMIP6 Forcing

**Holger Pohlmann[1,2], Wolfgang A. Müller[1], Matthias Bittner[1], Sebastian Hettrich[1], Kameswarrao Modali[1], Klaus Pankatz[2], and Jochem Marotzke[1]**

[1]Max-Planck-Institut für Meteorologie, Hamburg, Germany, [2]Deutscher Wetterdienst, Offenbach, Germany

**Abstract** We analyze the quasi-biennial oscillation (QBO) variability of historical and decadal hindcast simulations of the MiKlip (Mittelfristige Klimavorhersagen) decadal prediction system using the higher resolved version of the Max Planck Institute Earth System Model. We find a realistic variability of the QBO in historical simulations when changing from the Coupled Model Intercomparison Project Phase 5 (CMIP5) to the Coupled Model Intercomparison Project Phase 6 (CMIP6) external forcing. This agreement between the simulated and the observed QBO is improved by the initialization of decadal hindcast simulations with CMIP6 forcing in the first three lead years. In the decadal hindcast simulations, the agreement is similar to a persistence forecast in the first five lead years and higher than the persistence forecast in the later lead years. We find a strong relation between the QBO and the ozone variability in the stratosphere and conclude that the change of the ozone data from CMIP5 to CMIP6 leads to the improved QBO variability and prediction skill in our simulations.

**Plain Language Summary** The quasi-biennial oscillation (QBO) is a climate mode in the stratosphere with the feature of reversing wind directions above the equator roughly every second year (period of 28 months). The QBO variability has worldwide implications for other climate modes like the strength of the polar vortex that influences Europe via the North Atlantic Oscillation. Previous historical simulations with our climate model show that with a high vertical resolution, the model is able to produce a QBO variability, however, with an unrealistic phase. These historical simulations need external forcing like greenhouse gases and ozone concentrations. We show that in our simulations, the QBO variability becomes realistic when we use the updated external forcing data from Coupled Model Intercomparison Project Phase 6 (CMIP6) instead of those from CMIP5. Moreover, we find evidence that the variability of the stratospheric ozone data leads to the realistic QBO variability in our climate simulations. This has implications for decadal climate predictions since—for a good climate prediction—the stratospheric ozone variability must be projected into the future.

## 1. Introduction

The QBO is the dominant mode of variability in the tropical stratosphere. The characteristic of the QBO is a downward propagation of wind reversals (changing from easterly to westerly directions and vise versa) with a periodicity of about 28 months (Baldwin et al., 2001). The QBO has an effect on the strength of the polar vortex and hence can influence tropospheric variability such as the Northern Annular Mode and the North Atlantic Oscillation via the Holton-Tan mechanism (Holton & Tan, 1980; Thompson et al., 2002).

The QBO is predictable on seasonal timescales (Boer & Hamilton, 2008). Nowadays, the vertical resolution in many climate models is high enough to allow for a freely evolving QBO variability (Giorgetta et al., 2006), which is a prerequisite for the QBO predictability. The QBO initiative (Butchart et al., 2018) systematically analyzes the representation of the QBO in different climate models. The QBO initiative diagnoses the QBO variability and its teleconnections from the Atmospheric Model Intercomparison Project (Gates et al., 1998) simulations with present day and increased $CO_2$ levels and hindcast (i.e. retrospective forecast) simulations (e.g., Osprey et al., 2018) and underlines the importance of the QBO for the climate variability.

The analysis of the time horizon for skillful QBO predictions has shown predictability of more than 3 years in decadal climate prediction systems (Pohlmann et al., 2013; Scaife et al., 2014). In this study, we show that the update in higher resolved version of the Max Planck Institute Earth System Model (MPI-ESM-HR) historical simulations (Mauritsen et al., 2019; Müller et al., 2018) and decadal hindcast simulations with the MiKlip decadal climate prediction system (Marotzke et al., 2016) from Coupled Model Intercomparison Project Phase 5 (CMIP5; Taylor et al., 2012) to CMIP6 (Eyring et al., 2016) external forcing data leads to a realistic QBO variability.

## 2. The MiKlip Decadal Prediction System

We use the MPI-ESM-HR (Mauritsen et al., 2019; Müller et al., 2018) together with the historical simulations using CMIP5 (Taylor et al., 2012) and CMIP6 (Eyring et al., 2016) forcing. MPI-ESM-HR uses the European Centre Hamburg version 6.3 (ECHAM6.3) as the atmospheric component with a resolution of T127L95 (~100 km in the horizontal with 95 vertical levels) and the Max Planck Institute ocean model as the oceanic component of TP0.4 (0.4° nominal) resolution. The increase of the atmospheric horizontal model resolution leads to an improved atmospheric circulation in the extratropics (Müller et al., 2018). We compare our results also to the previous MiKlip hindcast system MPI-ESM-MR of T63L95 (~200 km in the horizontal with 95 vertical levels) resolution (Pohlmann et al., 2013). The high vertical resolution of the MPI-ESM-MR (i.e., the same as in MPI-ESM-HR) climate model is needed to allow a spontaneous QBO variability (Schmidt et al., 2013). To answer the question whether the achieved skill of the predicted QBO is in the range of what is expected, we compare our results also to a statistical model that uses a simple sinusoidal function with a period of 28 months, as suggested by Scaife et al. (2014).

The historical simulations with MPI-ESM-HR are analyzed in Müller et al. (2018) and Mauritsen et al. (2019). In the following, we describe the MiKlip decadal prediction system employing the MPI-ESM-HR climate model. The decadal hindcast simulations with MPI-ESM-HR are initialized every year from reanalysis data over the period 1960–2018. As in our previous system with MPI-ESM-MR (Pohlmann et al., 2013), the MPI-ESM-HR hindcasts are initialized from oceanic temperature and salinity anomalies from the European Centre for Medium Range Weather Forecasts (ECMWF) Ocean Reanalysis System 4 (ORAS4; Balmaseda et al., 2012) and atmospheric data (temperature, vorticity, divergence, and surface pressure) from ECMWF's 40-year Reanalysis (ERA40; Uppala et al., 2005) and ECMWF's interim Reanalysis (ERA-Interim; Dee et al., 2011). A new component in the initialization procedure is the initialization with sea-ice concentrations from the National Snow and Ice Data Center as described in Bunzel et al. (2016). The difference here is that we use anomalies instead of full-field values combined with a climatology before 1979 when no satellite observations are available. An ensemble of five members with CMIP6 forcing is produced for the Decadal Climate Prediction Project (Boer et al., 2016) by the Max Planck Institute for Meteorology (ensemble members r1–5), and another five ensemble members are performed by the Deutscher Wetterdienst (ensemble members r6–10). We compare our results to a five-member hindcast ensemble with CMIP5 forcing employing the same model MPI-ESM-HR. We also show the prediction skill from our previous MiKlip system (MPI-ESM-MR) consisting of five ensemble members, also forced by CMIP5 external boundary conditions, and a persistence forecast. The initialization of the hindcasts of the MPI-ESM-MR system starts at the end of 1960 and ends in 2012. We therefore choose the longest possible common period (i.e., 1970–2013) for the skill evaluation, for which all 10 lead years are available. We also compare our results to five ensemble members of historical simulations with MPI-ESM-HR and CMIP5 as well as CMIP6 forcing and with MPI-ESM-MR and CMIP5 forcing.

We define the QBO as the monthly and zonal mean zonal wind in the tropics averaged between 20°N–20°S at different height levels. We compare the QBO of our climate model simulations to the one from the ERA reanalysis, using ERA40 for the period 1960–1989 followed by ERA-Interim for the period 1990–2018. The MPI-ESM-HR systems are initialized in November of each year, while the MPI-ESM-MR system is initialized in January of each year. To be consistent with the definition of the lead year, the first 2 months are neglected in our analysis of the MPI-ESM-HR systems. Note that the start month can have an influence on the prediction skill (Scaife et al., 2014).

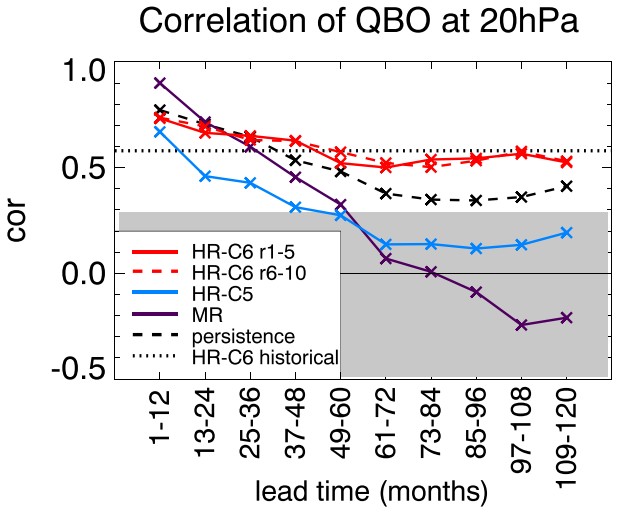


**Figure 1.** QBO correlation skill at different lead times for the ensemble mean of members r1–5 (red) and r6–10 (red dashed) of the MPI-ESM-HR system with CMIP6 external forcing, the five ensemble members of the MPI-ESM-HR system with CMIP5 external forcing (blue), the three ensemble members of the MPI-ESM-MR system with CMIP5 external forcing (purple), the persistence forecast using a simple sinusoidal function with a period of 28 months (black dashed), and the ensemble mean of five historical MPI-ESM-HR simulations with CMIP6 forcing (black dotted) at the 20-hPa height level. Outside of the grey area, the correlation values are significant at the 95% level according to a *t* test.

## 3. Forcing Data

CMIP organizes the coordinated climate simulations that are assessed in the Assessment Reports (AR) of the Intergovernmental Panel on Climate Change. For the coordinated experiments, CMIP6 (Eyring et al., 2016) provides updated forcing data. Information about the CMIP5 forcing is available from the AR5 of the Intergovernmental Panel on Climate Change (Myhre et al., 2013). In the following, we summarize the changes in the CMIP6 forcing relevant for our experiments.

Historical greenhouse gas concentrations (global annual means of $CO_2$, $CH_4$, $N_2O$, CFC-11, and CFC-12) from the University of Melbourne (UoM-CMIP-1-2-0; Meinshausen et al., 2017) are used for the CMIP6 simulations. In contrast to CMIP5, the greenhouse gases in CMIP6 are latitudinally and seasonally resolved. However, as was done with the CMIP5 forcing, with MPI-ESM-HR, we only use global and annual mean values to be comparable with these. The greenhouse gas concentrations used for the CMIP5 and CMIP6 simulations are very similar (supporting information Figure S1).

For the simulations with CMIP6 forcing, merged ozone fields from the Chemistry-Climate Model Initiative (Morgenstern et al., 2017) within the Whole Atmosphere Community Climate Model (Marsh et al., 2013) and the Canadian Middle Atmosphere Model (Scinocca et al., 2008) ozone simulations are used (Williams et al., 2019). In contrast to CMIP5, the ozone forcing in CMIP6 is regionally resolved. However, with MPI-ESM-HR, we use zonal mean values to be consistent with the CMIP5 forcing. The total column ozone values are slightly lower with increased variability in the CMIP6 forcing compared to CMIP5 (Figure S2).

The solar irradiation data from CMIP6 are prescribed in MPI-ESM-HR in the same way as previously done with the CMIP5 data. The total solar irradiation (TSI) includes secular trends as well as the 11-year solar cycle and is distributed over 14 spectral bands (Giorgetta et al., 2013). The irradiance of each band can vary with time independently (Schmidt et al., 2013). For the CMIP6 experiments, the solar forcing is derived as described in Matthes et al. (2017). The TSI is approximately 1,361 W/m$^2$ with slightly smaller maxima in the CMIP6 forcing compared to CMIP5 before 1880 and after 1980 (Figure S3).

Volcanic stratospheric aerosol forcing based on satellite data (Thomason et al., 2018; Zanchettin et al., 2017) are used for the CMIP6 simulations. The volcanic aerosol data show large differences to the previous data from CMIP5. Especially in the early period, the aerosol optical depth values are lower in the CMIP6 compared to the CMIP5 forcing (Figure S4). The anthropogenic aerosol optical properties from the second version (v2) of the Max Planck Institute Aerosol Climatology (MACv2-SP; Stevens et al., 2016) are used for the simulations with CMIP6 forcing. A new version of data from the Land-Use Harmonization version LUH2v2h (Li et al., 2018) is used as forcing for the MPI-ESM-HR simulations with CMIP6 forcing.

## 4. Results

The QBO (at 20 hPa) prediction skill (correlation) between the ERA reanalysis and climate simulations (ensemble mean of five ensemble members) is presented in Figure 1. We have derived robust results for the QBO analysis at the 10-, 20-, and 30-hPa levels and choose the intermediate level for displaying the results in this study. At lower levels, the results are not as robust, because there is still an issue forecasting the descent of the QBO. The historical simulations with MPI-ESM-HR with CMIP6 forcing are statistically significantly correlated (cor = 0.59) with the reanalysis data over the period 1970–2013 (and cor = 0.62 over the period 1970–2005). This high correlation is not achieved in historical simulations with the MPI-ESM-HR system with CMIP5 forcing (cor = 0.12) and MPI-ESM-MR system (cor = 0.24) over the shorter period 1970–2005 (when the CMIP5 historical period ends).

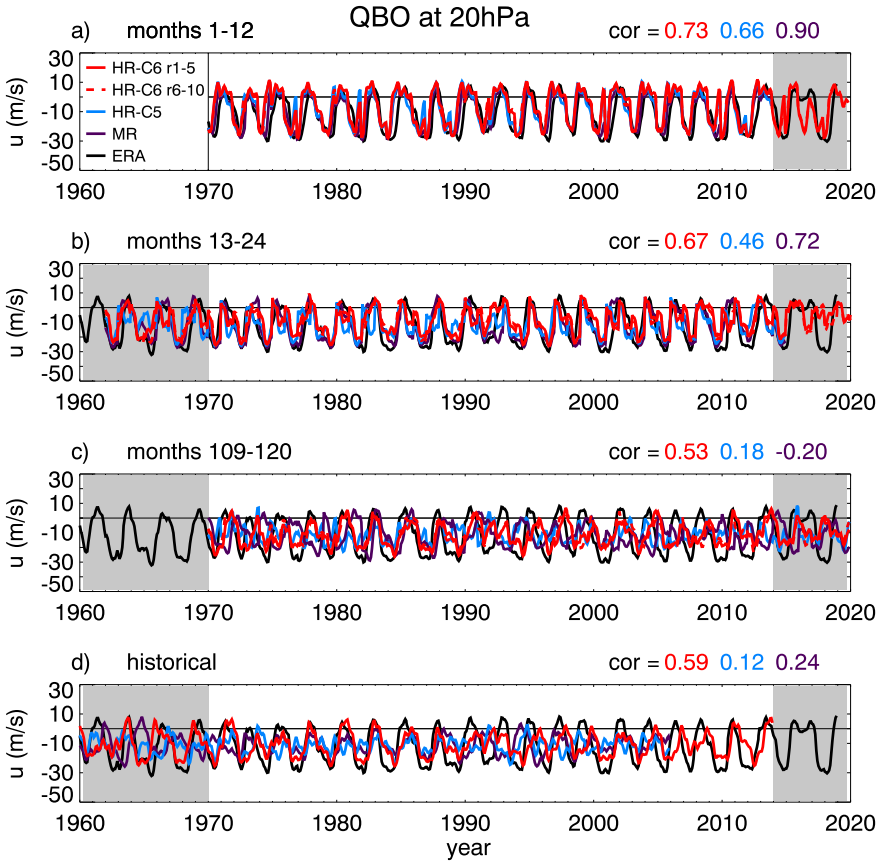


**Figure 2.** Concatenated time series of the QBO at 20 hPa at different lead times for the ensemble mean of members r1–5 (red) and r6–10 (red dashed) of the MPI-ESM-HR system with CMIP6 external forcing, the five ensemble members of the MPI-ESM-HR system with CMIP5 external forcing (blue), and the five ensemble members of the MPI-ESM-MR system with CMIP5 external forcing (purple) for lead months (a) 1–12, (b) 13–24, and (c) 109–120. The grey areas limit the period for which the QBO prediction skill in Figure 1 is calculated (1970–2013). (d) The time series of the QBO at 20 hPa of the ensemble mean of five historical simulations with MPI-ESM-HR with CMIP6 forcing (red) and MPI-ESM-HR with CMIP5 forcing (blue) as well as three ensemble members of MPI-ESM-MR (purple). Additionally, the numbers above each figure show correlation skill for the first five ensemble members of MPI-ESM-HR with CMIP6 forcing, MPI-ESM-HR with CMIP5 forcing, and MPI-ESM-MR.

The QBO of the hindcast simulations with the HR-CMIP6 system has a similar correlation skill as the persistence forecast in the first lead years. While the correlation skill of the persistence forecast drops below the one from the historical simulations, the correlation skill is maintained in the hindcast simulations for the later 6–10 lead years (61–120 lead months). The similarity between the two 5-member ensembles from HR-CMIP6 hindcasts (red curves in Figure 1) demonstrates the robustness of our results. The QBO correlation skill of the HR-CMIP5 system has similar values as the HR-CMIP6 system in the first part of the forecasts, but the correlation skill rapidly falls below the significance level after only three lead years (36 lead months). The MPI-ESM-MR system starts from a higher correlation value than the MPI-ESM-HR and drops below the significance level after about four lead years (48 lead months). The initialization of the MPI-ESM-HR systems in November instead of January in the MPI-ESM-MR system could cause the difference in the initial correlation values (Scaife et al., 2014).

The concatenated QBO (at 20 hPa) time series of the different systems and different lead times are shown in Figure 2. For the first 12 lead months, all simulated QBO time series show a high correlation with the QBO in the ERA reanalysis (cor = 0.73, 0.66, and 0.90 for HR-CMIP6, HR-CMIP5, and MR, respectively). For the lead months 13–24, the correlation of all simulated QBO time series with the one from ERA reanalysis data is also high (cor = 0.67, 0.46, and 0.72 for HR-CMIP6, HR-CMIP5, and MR, respectively. At lead months 109–120, the correlation of the QBO in the HR-CMIP6 system with the ERA reanalysis data is

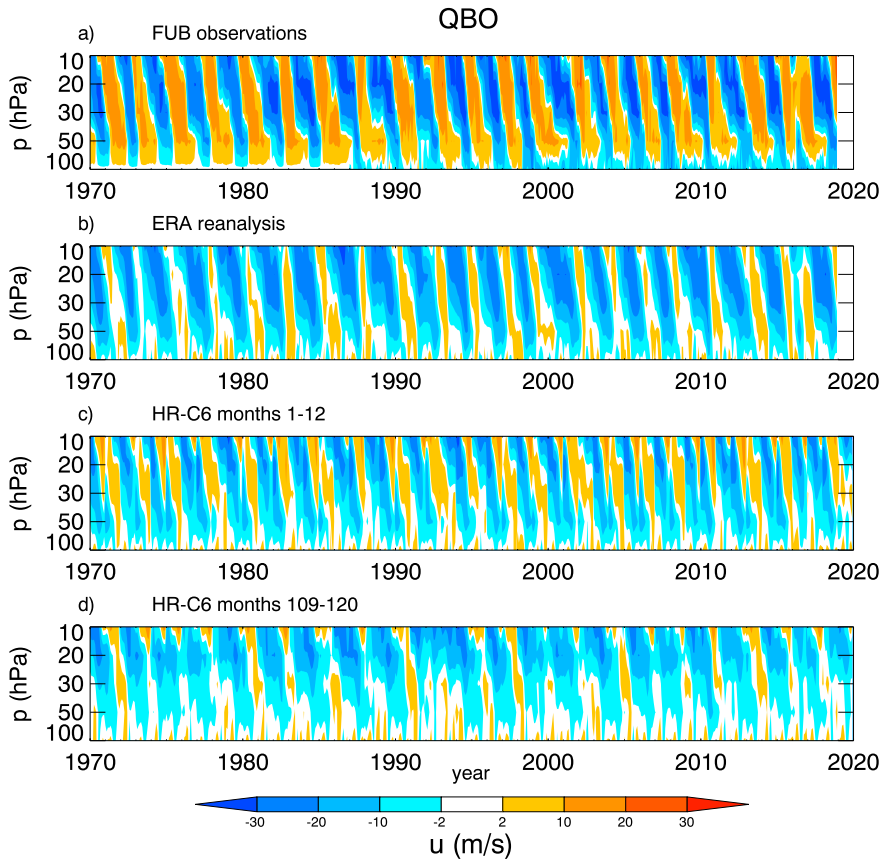


**Figure 3.** Hovmöller (time/height) diagram of the QBO (m/s) from (a) FUB observations and (b) ERA reanalysis and ensemble mean of members r1–5 of MPI-ESM-HR with CMIP6 external forcing for lead months (c) 1–12 and (d) 109–120. Note that for (b)–(d) the zonal mean zonal wind is averaged between 20°N and 20°S.

still high (cor = 0.53). At this lead time, neither the QBO of the HR-CMIP5 system (cor = 0.18) nor the QBO of the MR system (cor = −0.20) have a correlation with the ERA reanalysis data that is above the level for being significant at the 95% level according to a *t* test (i.e., values above 0.30). Additionally, the QBO time series of the historical simulations are shown for completeness. The QBO time series of the historical simulations with MPI-ESM-HR with CMIP6 forcing is significantly correlated (cor = 0.59) with the one from ERA reanalysis. Both the MPI-ESM-HR historical simulations with CMIP5 forcing (cor = 0.12) and the MPI-ESM-MR historical simulations (cor = 0.24) have lower (insignificant) correlation.

The height- and time-dependent QBO is presented in a Hovmöller diagram in Figure 3. For this comparison, we show the observed QBO as combined radiosonde data from Canton Island, Gan/Maldive Islands, and Singapore from the Freie Universität Berlin (Figure 3). We also show the ERA reanalysis data, since we have recognized that our system is better able to forecast the QBO averaged over the broader tropics (20°S–20°N) than for smaller ranges closer to certain locations. It becomes clear from Figure 3 that the averaged zonal wind (as for the ERA reanalysis) is quite different to the station observations (as for the Freie Universität Berlin data) and that therefore we should compare our simulations to the more complete ERA reanalysis. In the ERA reanalysis, the easterly phase of the QBO is more pronounced; over a longer duration, the westerly phase is almost absent. In the HR-CMIP6 system, the QBO with lead months 1–12 generally has an easterly bias, although the phase corresponds quite well with the one of the ERA reanalysis. At lead months 109–120, the easterly bias is also present, and the QBO does not reach as far down as in the ERA reanalysis or with lead months 1–12. The interrupted downward propagation of the QBO at this lead time may hamper the signal propagation and feedbacks.

The height- and time-dependent deviation of the QBO period from 28 months is presented in Figure 4. In the HR-CMIP6 system for lead months 1–12 and also lead months 109–120, the deviation pattern bears some

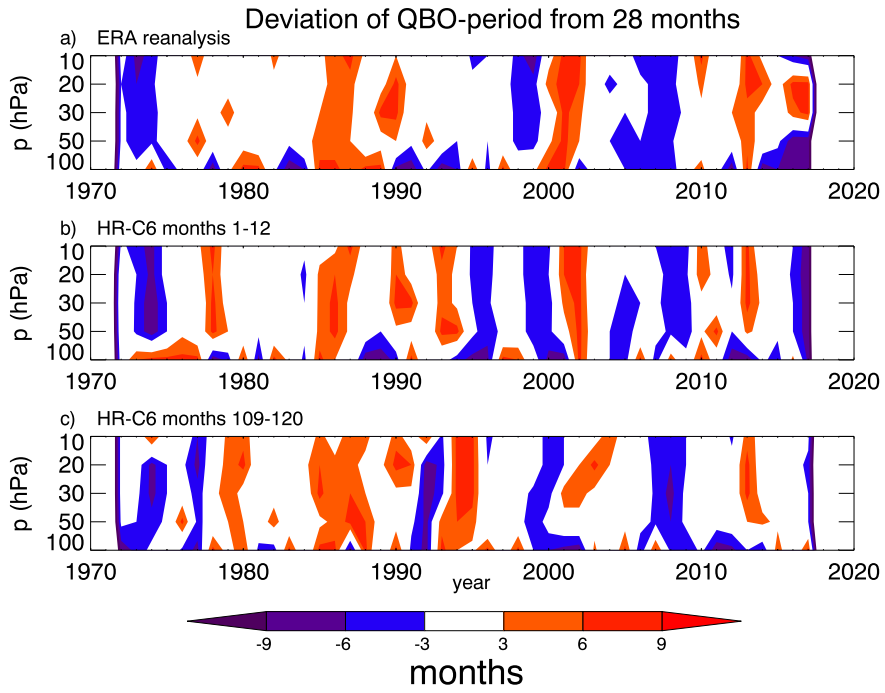


**Figure 4.** Hovmöller (time/height) diagram of the deviation of the QBO period from 28 months from (a) ERA reanalysis and ensemble mean of members r1–5 of MPI-ESM-HR with CMIP6 external forcing for lead months (b) 1–12 and (c) 109–120.

similarity to the pattern in the ERA reanalysis. The strongest differences appear at the 100-hPa level. The deviation pattern of the HR-CMIP5 system and also the MR system is very different to the pattern in the ERA reanalysis for the longer lead times (not shown).

Next, we want to answer the question why the update of the external forcing from CMIP5 to CMIP6 leads to a realistic QBO in simulations with the MPI-ESM-HR climate model. The update of the external forcing includes all components, that is, greenhouse gases, anthropogenic and volcanic aerosols, ozone, solar irradiation, and land use. While all of these forcing data could have an impact on the climate simulations, ozone has the strongest relation to the stratospheric temperature and hence can influence the stratospheric circulation. Therefore, we calculate the correlation between the QBO (at 20 hPa) and the zonal mean ozone time series at different height levels (Figure 5). At the equator, we find a significant correlation of the QBO with ozone at 20-hPa level (cor = 0.46) but even higher correlation values to the ozone at 30 hPa (cor = 0.80). Such high values are not present when the QBO is correlated with the ozone data from CMIP5 (not shown), which has correlation values only in the range of [−0.16, 0.13] for the different levels and latitudes. We therefore conclude that the change of the ozone data from CMIP5 to CMIP6 leads to the improved QBO variability in our simulations.

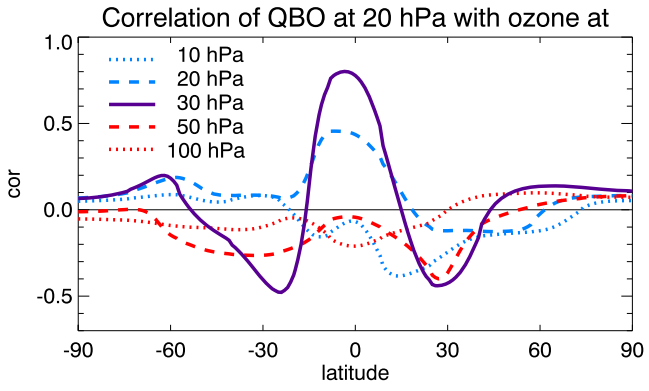


**Figure 5.** Correlation of the QBO at 20 hPa from the ERA reanalysis with the time series of ozone from CMIP6 at different latitudes and height levels.

## 5. Conclusions

We analyze historical simulations with the MPI-ESM-HR climate model and find a realistic QBO variability when changing from CMIP5 to CMIP6 external forcing. In decadal hindcast simulations with the MiKlip system employing the MPI-ESM-HR model with CMIP6 forcing, the agreement of QBO variability with ERA reanalysis data is maintained over the decadal timescale. The initialization of decadal hindcasts in the MiKlip system increases the correlation skill further compared to historical simulations in the first three lead years.

However, we have also shown deficiencies of the vertical structure of the predicted QBO. The easterly component of the QBO in the MPI-ESM-HR climate model is in general too strong. Additionally, in the later prediction years, the downward propagation of QBO variability is interrupted and may therefore hamper teleconnections and feedbacks.

While the update of all components of the CMIP forcing could potentially lead to different results in the climate simulations with MPI-ESM-HR, ozone bears the strongest relation to the stratospheric temperature and hence can influence the stratospheric circulation by horizontally and vertically displacing the circulation regimes. We find a strong correlation between QBO at 20 hPa from the ERA reanalysis and ozone variability in the CMIP6 data at the level below (30 hPa), a correlation that is not present using the CMIP5 data. We conclude therefore that the change of the ozone data from CMIP5 to CMIP6 leads to the realistic QBO variability in our simulations with the MPI-ESM-HR climate model. Although the correlation of the QBO with other external forcing data (like AOD and TSI) is close to zero, these may also contribute to the QBO variability during certain periods.

For a good climate prediction over the coming 10 years, known issues that need to be addressed are that the solar irradiation must be projected into the future and that there are unpredictable risks of volcanic eruptions causing climate disruptions. Additionally, the QBO must be projected into the future. Our persistence forecast using a simple sinusoidal function can project the QBO up to 5 years into the future but has deficiencies at longer timescales. The MiKlip decadal prediction system has a similar QBO correlation skill in the first lead years as the persistence forecast and is able to maintain the correlation of the historical simulations in the later lead years. Our study demonstrates that the QBO can be predicted with a decadal climate prediction system on the multiannual timescale but that the prediction is also dependent on the ozone external forcing data.

**Acknowledgments**
The research leading to these results has received funding from the German Federal Ministry for Education and Research (BMBF) project MiKlip (http://www.fona-miklip.de). This study uses ECMWF reanalysis data from ERA40, ERA-Interim, and ORAS4 (https://www.ecmwf.int). QBO observations are obtained from the Freie Universität Berlin (https://www.geo.fu-berlin.de/en/met/ag/strat/produkte/qbo/index.html). The climate simulations were performed at the German Climate Computing Centre (DKRZ). Data and scripts used in this study will be made available from the Climate and Environmental Retrieval and Archive (CERA) of the World Data Center for Climate (https://www.dkrz.de/up/systems/wdcc). The authors thank Dian Putrasahan and two anonymous reviewers whose comments helped to improve a former version of this paper.

## References

Baldwin, M. P., Gray, L. J., Dunkerton, T. J., Hamilton, K., Haynes, K., Randel, W. J., et al. (2001). The quasi-biennial oscillation. *Reviews of Geophysics*, *39*(2), 179–229. https://doi.org/10.1029/1999RG000073

Balmaseda, M. A., Mogensen, K., & Weaver, A. T. (2012). Evaluation of the ECMWF ocean reanalysis system. *Quarterly Journal of the Royal Meteorological Society*, *139*, 1132–1161. https://doi.org/10.1002/qj.2063

Boer, G., & Hamilton, K. (2008). QBO influence on extratropical predictive skill. *Climate Dynamics*, *31*, 987–1000. https://doi.org/10.1007/s00382-008-0379-5

Boer, G. J., Smith, D. M., Cassou, C., Doblas-Reyes, F., Danabasoglu, G., Kirtman, B., et al. (2016). The Decadal Climate Prediction Project. *Geoscientific Model Development*, *9*(10), 3751–3777. https://doi.org/10.5194/gmd-9-3751-2016

Bunzel, F., Notz, D., Baehr, J., Müller, W. A., & Fröhlich, K. (2016). Seasonal climate forecasts significantly affected by observational uncertainty of Arctic sea ice concentration. *Geophysical Research Letters*, *43*, 852–859. https://doi.org/10.1002/2015GL066928

Butchart, N., Anstey, J. A., Hamilton, K., Osprey, S., McLandress, C., Bushell, A. C., et al. (2018). Overview of experiment design and comparison of models participating in phase 1 of the SPARC Quasi-Biennial Oscillation initiative (QBOi). *Geoscientific Model Development*, *11*(3), 1009–1032. https://doi.org/10.5194/gmd-11-1009-2018

Dee, D. P., Uppala, S. M., Simmons, A. J., Berrisford, P., Poli, P., Kobayashi, S., et al. (2011). The ERA-Interim reanalysis: Configuration and performance of the data assimilation system. *Quarterly Journal of the Royal Meteorological Society*, *137*(656), 553–597. https://doi.org/10.1002/qj.828

Eyring, V., Bony, S., Meehl, G. A., Senior, C. A., Stevens, B., Stouffer, R. J., & Taylor, K. E. (2016). Overview of the Coupled Model Intercomparison Project Phase 6 (CMIP6) experimental design and organization. *Geoscientific Model Development*, *9*, 1937–1958. https://doi.org/10.5194/gmd-9-1937-2016

Gates, W. L., Boyle, J., Covey, C., Dease, C., Doutriaux, C., Drach, R., et al. (1998). An Overview of the results of the Atmospheric Model Intercomparison Project (AMIP I). *Bulletin of the American Meteorological Society*, *80*(1), 29–55. https://doi.org/10.1175/1520-0477(1999)080<0029:AOOTRO>2.0.CO;2

Giorgetta, M. A., Jungclaus, J., Reick, C. H., Legutke, S., Bader, J., Böttinger, M., et al. (2013). Climate and carbon cycle changes from 1850 to 2100 in MPI-ESM simulations for the Coupled Model Intercomparison Project phase 5. *Journal of Advances in Modeling Earth Systems*, *5*, 572–597. https://doi.org/10.1002/jame.20038

Giorgetta, M. A., Manzini, E., Roeckner, E., Esch, M., & Bengtsson, L. (2006). Climatology and forcing of the quasi-biennial oscillation in the MAECHAM5 model. *Journal of Climate*, *19*, 3882–3901. https://doi.org/10.1175/JCLI3830.1

Holton, J. R., & Tan, H.-C. (1980). The influence of the quasi-biennial oscillation on the global circulation at 50 mb. *Journal of the Atmospheric Sciences*, *37*, 2200–2208. https://doi.org/10.1175/1520-0469(1980)037<2200:TIOTEQ>2.0.CO;2

Li, W., MacBean, N., Ciais, P., Defourny, P., Lamarche, C., & Bontemps, et al. (2018). Gross and net land cover changes in the main plant functional types derived from the annual ESA CCI land cover maps (1992–2015). *Earth System Science Data*, *10*, 219–234. https://doi.org/10.5194/essd-10-219-2018

Marotzke, J., Müller, W. A., Vamborg, F. S. E., Becker, P., Cubasch, U., Feldmann, H., et al. (2016). MiKlip: A national research project on decadal climate prediction. *Bulletin of the American Meteorological Society*, *97*(12), 2379–2394. https://doi.org/10.1175/BAMS-D-15-00184.1

Marsh, D., Mills, M. J., Kinnison, D. E., Garcia, R. R., Lamarque, J.-F., & Calvo, N. (2013). Climate change from 1850–2005 simulated in CESM1 (WACCM). *Journal of Climate*, *26*, 7372–7391. https://doi.org/10.1175/JCLI-D-12-00558.1

Matthes, K., Funke, B., Andersson, M. E., Barnard, L., Beer, J., Charbonneau, P., et al. (2017). Solar forcing for CMIP6 (v3.2). *Geoscientific Model Development*, *10*(6), 2247–2302. https://doi.org/10.5194/gmd-10-2247-2017

Mauritsen, T., Bader, J., Becker, T., Behrens, J., Bittner, M., Brokopf, R., et al. (2019). Developments in the MPI-M Earth System Model version 1.2 (MPI-ESM 1.2) and its response to increasing $CO_2$. *Journal of Advances in Modeling Earth Systems*, *11*, 998–1038. https://doi.org/10.1029/2018MS001400

Meinshausen, M., Vogel, E., Nauels, A., Lorbacher, K., Meinshausen, N., Etheridge, D. M., et al. (2017). Historical greenhouse gas concentrations for climate modelling (CMIP6). *Geoscientific Model Development*, *10*(5), 2057–2116. https://doi.org/10.5194/gmd-10-2057-2017

Morgenstern, O., Hegglin, M., Rozanov, E., O'Connor, F. M., Abraham, L., Akiyoshi, H., et al. (2017). Review of the global models used within phase 1 of the Chemistry-Climate Model Initiative (CCMI). *Geoscientific Model Development*, *10*(2), 639–671. https://doi.org/10.5194/gmd-10-639-2017

Müller, W. A., Jungclaus, J. H., Mauritzen, T., Baehr, J., Bittner, M., Budich, R., et al. (2018). A higher-resolved version of the Max Planck Institute Earth System Model (MPI-ESM 1.2-HR). *Journal of Advances in Modeling Earth Systems*, *10*, 1383–1413. https://doi.org/10.1029/2017MS001217

Myhre, G., Shindell, D., Bréon, F.-M., Collins, W., Fuglestvedt, J., Huang, J., et al. (2013). Anthropogenic and natural radiative forcing. In T. F. Stocker, D. Qin, G.-K. Plattner, M. Tignor, S. K. Allen, J. Boschung, et al. (Eds.), *Climate change 2013: The physical science basis. Contribution of Working Group I to the Fifth Assessment Report of the Intergovernmental Panel on Climate Change* (Chap. 8, pp. 659–740). Cambridge, United Kingdom and New York, NY, USA: Cambridge University Press.

Osprey, S., Geller, M., & Yoden, S. (2018). The stratosphere and its role in tropical teleconnections. *Earth and Space Science News*, *99*. https://doi.org/10.1029/2018EO097387

Pohlmann, H., Müller, W. A., Kulkarni, K., Kameswarrao, M., Matei, D., Vamborg, F. S. E., et al. (2013). Improved forecast skill in the tropics in the new MiKlip decadal climate predictions. *Geophysical Research Letters*, *40*, 5798–5802. https://doi.org/10.1002/2013GL058051

Scaife, A. A., Athanassiadou, M., Andrews, M., Arribas, A., Baldwin, M., Dunstone, N., et al. (2014). Predictability of the quasi-biennial oscillation and its northern winter teleconnection on seasonal to decadal timescales. *Geophysical Research Letters*, *41*, 1752–1758. https://doi.org/10.1002/2013GL059160

Schmidt, H., Rast, S., Bunzel, F., Esch, M., Giorgetta, M., Kinne, S., et al. (2013). Response of the middle atmosphere to anthropogenic and natural forcings in the CMIP5 simulations with the Max Planck Institute Earth system model. *Journal of Advances in Modeling Earth Systems*, *5*, 98–116. https://doi.org/10.1002/jame.20014

Scinocca, J. F., McFarlane, N. A., Lazare, M., Li, J., & Plummer, D. (2008). The CCCma third generation AGCM and its extension into the middle atmosphere. *Atmospheric Chemistry and Physics*, *8*, 7055–7074. https://doi.org/10.5194/acp-8-7055-2008

Stevens, B., Fiedler, S., Kinne, S., Peters, K., Rast, S., Müsse, J., et al. (2016). MACv2-SP: A parameterization of anthropogenic aerosol optical properties and an associated Twomey effect for use in CMIP6. *Geoscientific Model Development*, *10*(1), 433–452. https://doi.org/10.5194/gmd-10-433-2017

Taylor, K. E., Stouffer, R. J., & Meehl, G. A. (2012). An overview of CMIP5 and the experiment design. *Bulletin of the American Meteorological Society*, *93*, 485–498. https://doi.org/10.1175/BAMS-D-11-00094.1

Thomason, L. W., Ernest, N., Millán, L., Rieger, L., Bourassa, A., Vernier, J.-P., et al. (2018). A global space-based stratospheric aerosol climatology: 1979–2016. *Earth System Science Data*, *10*(1), 469–492. https://doi.org/10.5194/essd-10-469-2018

Thompson, D. W. J., Baldwin, M. P., & Wallace, J. M. (2002). Stratospheric connection to Northern Hemisphere wintertime weather: Implications for prediction. *Journal of Climate*, *15*, 1421–1428. https://doi.org/10.1175/1520-0442(2002)015<1421:SCTNHW>2.0.CO;2

Uppala, S. M., KÅllberg, P. W., Simmons, A. J., Andrae, U., Da Costa Bechtold, V., Fiorino, M., et al. (2005). The ERA-40 re-analysis. *Quarterly Journal of the Royal Meteorological Society*, *131*(612), 2961–3012. https://doi.org/10.1256/qj.04.176

Williams, R. S., Hegglin, M. I., Kerridge, B. J., Jöckel, P., Latter, B. G., & Plummer, D. A. (2019). Characterising the seasonal and geographical variability in tropospheric ozone, stratospheric influence and recent changes. *Atmospheric Chemistry and Physics*, *19*, 3589–3620. https://doi.org/10.5194/acp-19-3589-2019

Zanchettin, D., Khodri, M., Timmreck, C., Toohey, M., Schmidt, A., Gerber, E. P., et al. (2017). The Model Intercomparison Project on the climatic response to Volcanic forcing (VolMIP): Experimental design and forcing input data for CMIP6. *Geoscientific Model Development*, *9*(8), 2701–2719. https://doi.org/10.5194/gmd-9-2701-2016